Icarus **144**, 382–396 (2000)
doi:10.1006/icar.1999.6300, available online at http://www.idealibrary.com on IDEAL®

Variability of Mars' North Polar Water Ice Cap

I. Analysis of Mariner 9 and Viking Orbiter Imaging Data

Deborah S. Bass

Instrumentation and Space Research Division, Southwest Research Institute, P.O. Drawer 28510, San Antonio, Texas 78228-0510
E-mail: dsb@kronos.space.swri.edu

Kenneth E. Herkenhoff

U.S. Geological Survey, 2255 North Gemini Drive, Flagstaff, Arizona 86001

and

David A. Paige

Department of Earth and Space Sciences, University of California, Los Angeles, 405 Hilgard Avenue, Los Angeles, California 90095-1567

Received May 15, 1998; revised November 17, 1999

Previous studies interpreted differences in ice coverage between Mariner 9 and Viking Orbiter observations of Mars' north residual polar cap as evidence of interannual variability of ice deposition on the cap. However, these investigators did not consider the possibility that there could be significant changes in the ice coverage within the northern residual cap over the course of the summer season. Our more comprehensive analysis of Mariner 9 and Viking Orbiter imaging data shows that the appearance of the residual cap does not show large-scale variance on an interannual basis. Rather we find evidence that regions that were dark at the beginning of summer look bright by the end of summer and that this seasonal variation of the cap repeats from year to year. Our results suggest that this brightening was due to the deposition of newly formed water ice on the surface.

We find that newly formed ice deposits in the summer season have the same red-to-violet band image ratios as permanently bright deposits within the residual cap. We believe the newly formed ice accumulates in a continuous layer. To constrain the minimum amount of deposited ice, we used observed albedo data in conjunction with calculations using Mie theory for single scattering and a delta-Eddington approximation of radiative transfer for multiple scattering. The brightening could have been produced by a minimum of (1) a ∼35-μm-thick layer of 50-μm-sized ice particles with 10% dust or (2) a ∼14-μm-thick layer of 10-μm-sized ice particles with 50% dust.

Key Words: **Mars; Mars, Surface; Mars, Atmosphere; Mars, Climate; Surfaces, Planets.**

1. INTRODUCTION

Like Earth, Mars has perennial ice caps and an active water cycle. The Viking Orbiter determined that the surface of the northern residual cap is water ice (Kieffer *et al*. 1976, Farmer *et al*. 1976). At the south residual polar cap, both Mariner 9 and Viking Orbiter observed carbon dioxide ice throughout the summer. Many have related observed atmospheric water vapor abundances to seasonal exchange between reservoirs such as the polar caps, regolith adsorption, and cloud coverage (e.g., Jakosky and Farmer 1982, Kieffer 1990, Zent *et al*. 1986, Kahn 1990), but the extent and nature of martian surface and subsurface reservoirs and the extent to which they exchange between the surface and the atmosphere remain uncertain. In this paper, we examine Mariner 9 and Viking Orbiter imaging observations of the north residual polar cap to provide additional constraints on Mars' water cycle.

The cycles and variation of Mars' climate has been of interest for many years. Geologic evidence such as the dendritic valley networks (in addition to the outflow channels) on Mars has lead many to speculate that Mars' climate was much different in its past (e.g., Fanale *et al*. 1992). Further, there has been much discussion of martian climate change due to astronomical variations of the Mars' orbit and the orientation of its spin axis over million-year time scales (e.g., Bills 1990, Ward 1992, Touma and Wisdom 1993). It is the combination of the obliquity and the inclination of the martian orbit that produces very

0019-1035/00 $35.00

strong variations in solar insolation over the course of millions of years; such variations are most likely imprinted in the geological history of the planet. Any variations in the martian climate may be magnified by the variable nature of Mars' global dust storms (e.g., Kahn *et al*. 1992; Zurek and Martin 1993). However, to date there is no conclusive evidence documenting the cyclic nature of Mars' climate. Inferred climate change from layered ice cores on Earth (Jouzel *et al*. 1987) suggests that the record of Mars' climate variation is also likely recorded in layered polar ice. In the polar regions of Mars, high-resolution Mariner 9 and Viking images recorded a layered geologic unit (e.g., Cutts *et al*. 1970). The presence of the layered deposits has been widely attributed to climatically driven cycles of deposition and erosion of airborne dust and water ice due to quasiperiodic variations of Mars' orbital and axial elements (Ward 1992, Murray *et al*. 1973). These polar layered terrains may be the best recorders of martian global climate variability. A key to understanding whether the polar regions contain this record of Mars' climate history lies in assessing the rate at which the polar caps are currently gaining or losing mass. Further, comparing the simpler martian climate system to Earth's more complex one may lend insight into the mechanisms of climate change (Imbrie 1982). Finally, because the polar caps are currently large reservoirs of the volatiles involved in recent climate dynamics, examining changes in the polar cap appearance is a key to understanding recent climate change on Mars.

This investigation is divided into two parts. In this paper, we examine and interpret Mariner 9 and Viking Orbiter imaging data to place constraints on the interannual and/or seasonal variations in the appearance of Mars' north residual polar cap. We also model the minimum amount of ice potentially deposited on the cap surface using Mie theory for single scattering and a delta-Eddington approximation for multiple scattering. In a companion paper Bass and Paige (2000), we correlate the results of this paper with Viking Infrared Thermal Mapper data and Mars Atmospheric Water Detector data for a clearer picture of the processes involved in the martian north polar water cycle (Part II).

1.2. Spacecraft Observations

The current state of understanding of the martian polar caps and the global water cycle is primarily derived from spacecraft observations. In the fall and winter seasons, the polar regions are covered with seasonal carbon dioxide ice. The CO_2 ice sublimes in the spring, revealing the residual water ice cap in the north. We define the northern residual cap as the bright water ice cap that is visible in the summer season as well as the associated darker deposits that appear as curvilinear features in the residual cap and presumably underneath the residual cap. We define bright outliers to mean detached high albedo regions surrounding the main body of the residual cap. We define the term "ice" as the solid phase of any volatile regardless of its structure or formation process.

As atmospheric dust concentration theoretically affects the annual water cycle, previous investigators postulated a link between the cyclic deposition of water ice and dust onto the polar cap and the interannually occurring dust storms (e.g., James and Martin 1985, Kieffer 1990, Paige *et al*. 1994). Dust affects ice deposition in several ways: atmospheric dust decreases the albedo of the cap surface and increases sublimation. It also increases atmospheric temperatures and increases the water-holding capacity of the atmosphere. A thick dust layer deposited on a surface, however, can physically inhibit sublimation of surface CO_2 and H_2O ice and can act as an insulating layer on the cap surface (Hofstadter and Murray 1990).

2. MARINER 9 AND VIKING ORBITER IMAGING DATA

2.1. Previous Work

Previous investigators observed variance in the appearance of the north residual cap in Mariner 9 and Viking Orbiter imaging data. Calibration of Mariner 9 imaging data has been revisited in Herkenhoff *et al*. (1988), while Viking Orbiter calibration is presented in Klaasen *et al*. (1977). James and Martin (1985) looked at two consecutive summers of Viking observations and noted that a bright outlier that was visible in 1976 ($L_s = 135$) disappeared in 1978 ($L_s = 118$). (Areocentric solar longitude, or L_s, defines the martian season and measures the angle from the sun between Mars' current position and its position at the vernal equinox, i. e., $L_s = 0$ marks the vernal equinox and $L_s = 90$ marks the northern summer solstice.) Kieffer (1990) also made a similar observation: a comparison of data from two Viking summers showed the disappearance of a bright outlier from one year to the next. Paige *et al*. (1994) examined larger regions of the cap: a whole residual cap view provided by a Mariner 9 wide-angle frame ($L_s = 101$) compared to a Viking photomosaic ($L_s = 110$–155) taken 3 Mars years later showed much more bright ice in the Viking mosaic (Figs. 1a and 1b). Assuming that the seasonal cap decreases steadily throughout the spring and summer, global dust storms that occurred before the Mariner 9 observations were interpreted as causing decreased ice deposition following the storms and decreased cap brightness. It was noted that a global dust storm occurred in 1977 between the Viking observations mentioned in James and Martin (1985) and Kieffer (1990). These observations lead to the conclusion that the north polar cap net mass gain/loss rate varies interannually and that any changes in summertime cap appearance from one year to the next must also be due to some kind of variable deposition. As we will demonstrate, the observations interpreted as cap interannual variability are actually evidence supporting an unexpected appearance variation in the appearance of the cap that repeats each summer season.

2.2. Imaging Data Selection

Each image included in this study was acquired in the late northern spring or summer, from $L_s = 80$ to $L_s = 180$. The Viking

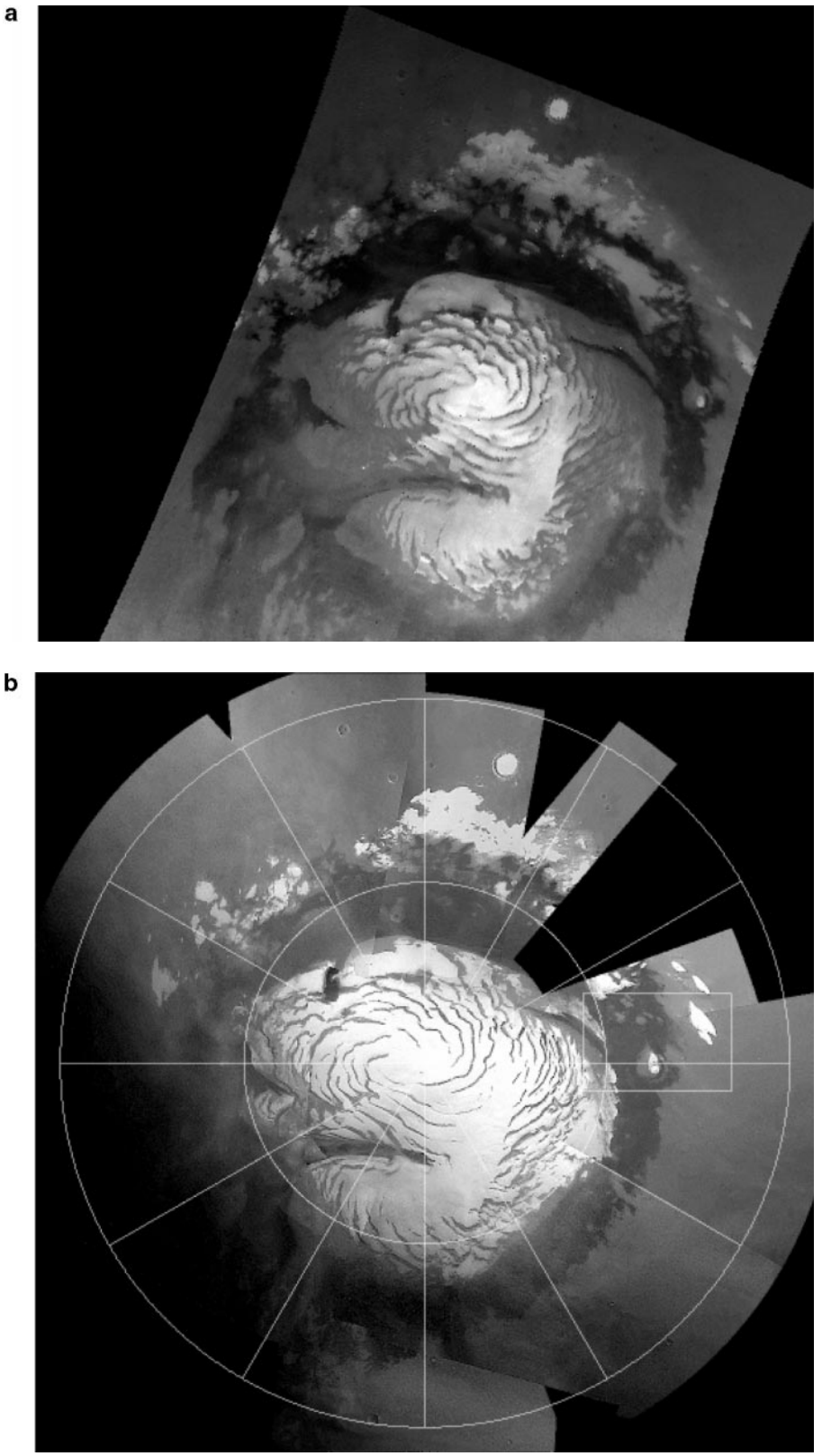

FIG. 1. Mars' residual north polar cap. (a) A Mariner 9 Orbiter wide-angle image of the north polar region of Mars, acquired at $L_s = 101$ in 1972 (668A10). Image is polar-projected and was corrected using a model Lambertian photometric correction function. The image was acquired 3 years before the Viking images in the full cap Viking photomosaic (b). Image shows less bright water ice than Viking image. Cap is approximately 1200 km across. (b) Viking Orbiter photomosaic of north residual cap, produced from USGS 256 m/pixel resolution images. The images were acquired between $L_s = 110$ and $L_s = 155$ in 1978, 3 Mars years after the full cap Mariner 9 Orbiter image (a). Image shows substantially more bright water ice, a finding which some thought suggested interannual variability of the water cycle. Rectangle in image outlines close-up region shown in Figs. 2a–2e.

Orbiter images used for this study were selected using Washington University's Image Retrieval and Processing System (IRPS). IRPS is an on-line database containing planetary images and imaging data product information. For more information about IRPS, see the *IRPS Software Specification Document* (Slavney and Guinness 1989). The results were compared to the archives at JPL's Regional Planetary Image Facility (RPIF), and images that did not appear in the IRPS search but still had data in the originally defined region were added to the final database, which totaled over 300 Viking Orbiter images. The Mariner 9 data were located using the image catalog contained in JPL Technical Memorandum 33-585 (Cutts 1974). The entire imaging database was examined for albedo variations, and a portion of the images with albedo variations has been selected for presentation here.

2.3. Imaging Data Processing

We utilized the USGS-developed Planetary Image Cartography System (PICS) to digitally process the imaging data. Data reduction in PICS is divided into four stages. Level 1 processing in PICS involves radiometric correction of the files. DN values are scaled to absolute radiometric units with respect to a Lambertian surface and a histogram of the DN values is created. The data are then filtered to despike the data. Level 2 processing includes procedures to geometrically control the images, in addition to procedures for the reprojection of rectilinear images to a wide variety of map projections, including sinusoidal equal area and polar stereographic. In this study all images were reprojected to polar stereographic projections. Level 3 processing involves matching resolutions between images and creating mosaics. Where possible, the images chosen for this study were mosaicked for broad-scale coverage. Level 4 processing reduces photometric inconsistencies by characterizing the photometry and then correcting according to model photometric functions. A summary of the procedures used to process each image in this study is found in Table I. Differences in illumination between images in this study were reduced using a Lambert scattering law, although no atmospheric corrections have been made. All images in this study were processed identically; therefore any artifacts introduced by the processing techniques would be introduced uniformly for all images. For more information about PICS, see *PICS—Planetary Image Cartography System*, version 1.1, United States Geological Survey, Flagstaff, Arizona, 1989. All images were finally stretched using a linear contrast, so that black $= 0$ DN, white $= 6000$ DN. The 16-bit data files were then converted to 8-bit files so that 6000 DN $= 255$. Note that DN $= 10{,}000 *$ Lambert albedo.

2.4. Imaging Data Results and Interpretations

Upon initial comparison of the Mariner 9 imaging data with published Viking mosaics, distinct differences in bright ice coverage consistent with earlier work (Bass *et al*. 1994, Paige *et al*. 1994, Kieffer 1990, James and Martin 1985) were noted. However, in depth examination showed that images acquired in different years but at approximately the same areocentric solar longitude have similar bright ice coverage. This similarity was noted for all the available Mariner 9 and Viking Orbiter data. For example, a Mariner 9 mosaic acquired at $L_s = 97$ in 1972 (Fig. 2a) has a similar amount of bright ice when compared to a Viking Orbiter mosaic (Fig. 2b) acquired 3 Mars years later but at a similar areocentric solar longitude ($L_s = 100$ in 1978). Observations reported by previous investigators as evidence for interannual variations in ice brightness are better interpreted as seasonal variations. Also, images acquired in two different years (1976 and 1978) during the Viking mission but at the same L_s show similar bright ice (Figs. 2d and 2e). These results contradict earlier conclusions that the northern residual polar cap exhibits readily apparent interannual variations in bright ice coverage. We suggest that earlier conclusions were reached because these studies compared images acquired during different years *and* different times in the summer. If there were large-scale interannual variability, there would be substantially different overall brightnesses in the compared images acquired in similar seasons.

To demonstrate the similarity of albedos measured at the same season during different years, we have differenced the imaging data. Figure 3 is the difference of Figs. 2d and 2e: two images acquired at very similar areocentric solar longitudes ($L_s = 134$

TABLE I

Procedure name	Input	Output
CD2PICS	Compressed EDR-formatted image, 8-bit image	PICS formatted image
SPICELAB	PICS formatted image with uncorrected label information	PICS formatted image with updated labels
LEVEL1	PICS 8-bit rectilinear image	16-bit, radiometrically corrected, cosmetically improved, and geometrically documented rectilinear image
BASE	16-Bit PICS image	Transformation "temporary" file ready to compare to base file
TVTIE	Transformation file and base image with known geometry	Geometrically registered PICS image
LEVEL2	PICS Level 1 geometrically registered image	Trimmed sinusoidal equal area map projected image
NUPROJ, GEOM	Sinusoidal equal area Level 2 image	Polar streographically projected image
PHOTOMPR, PHOTOM	Polar stereographic image	Photometrically corrected (Lambertian) image
DSK2DSK	Photometrically corrected image	Trimmed smaller image file
MOSAIC	Trimmed photometrically, radiometrically, and geometrically calibrated image files	Large mosaic of images

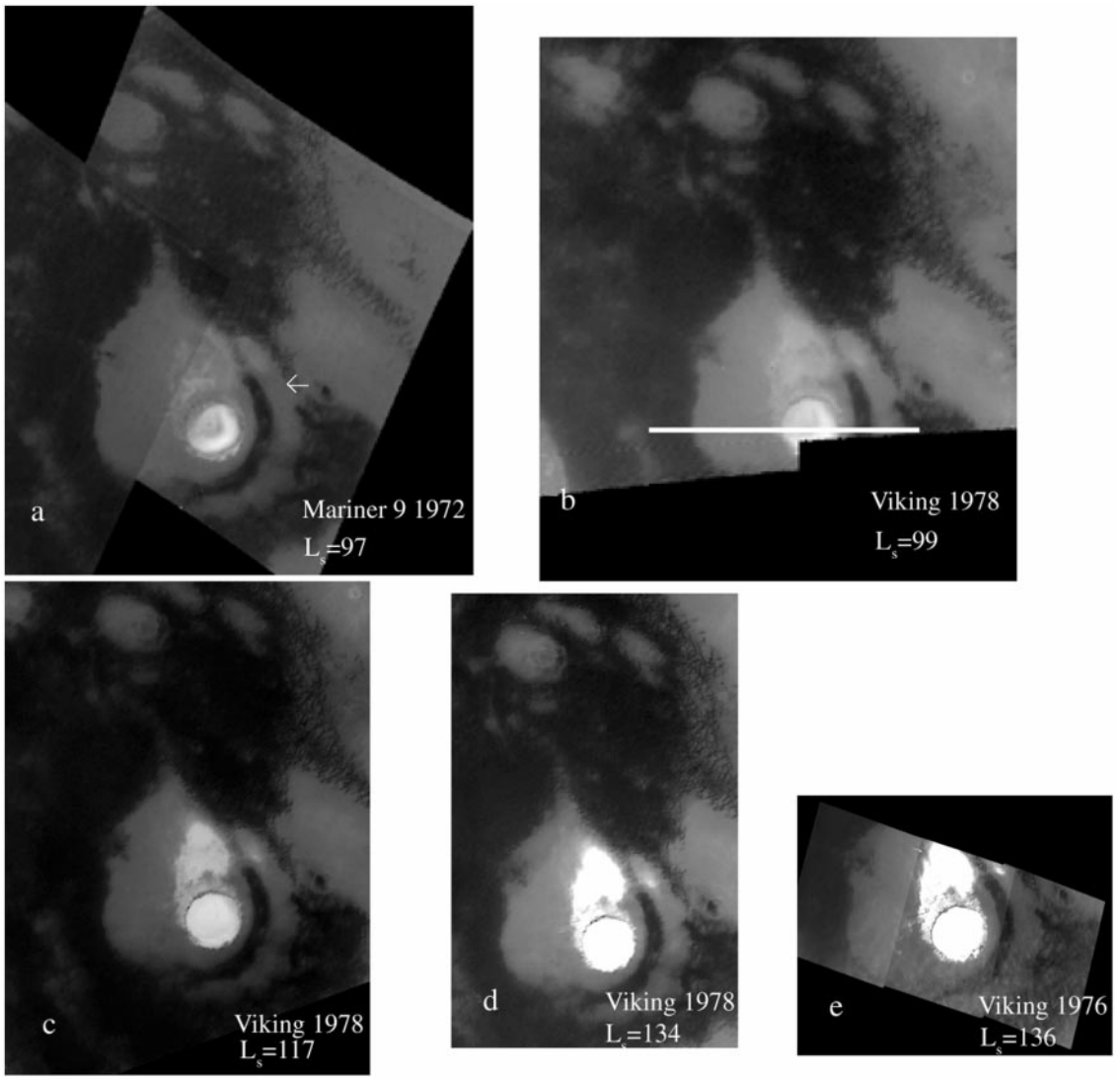

FIG. 2. Sequence of Mariner 9 and Viking images showing albedo increase with increasing areocentric solar longitude. Crater bowl is approximately 60 km in diameter. All images were acquired with red filters, except the Mariner 9, which was acquired with a minus-blue filter, and all images were corrected for illumination variations using a Lambertian model function. Sun direction for all images is from the lower right. A linear contrast stretch was employed for DN values between 0 and 3000 and then converted to values between 0 and 255, where 0 is black and 255 is white. DN = 10,000 ∗ Lambert albedo. (a) Mariner 9 mosaic of high-resolution polar images (675B57) acquired at $L_s = 97$ in 1972. Mosaic is centered at 85°N, 270°W. See Fig. 1b for the location of the data presented in Fig. 2. Sun direction is from the lower right. (b) Low-resolution Viking Orbiter mosaic (726A50, 726A52) from $L_s = 99$ shows similar ice coverage when compared with a Mariner 9 mosaic (Fig. 2a) of approximately the same region. White transect marks values used in quantitative albedo comparison (Fig. 5). (c) Viking Orbiter image (765A28) acquired at $L_s = 117$ shows more ice than earlier Mariner 9 (Fig. 2a) and Viking (Fig. 2b) images. Note distinct bright ice increase. (d) Low-resolution Viking Orbiter image (801A41) acquired approximately 40 days later ($L_s = 134$) than the image in Fig. 2c. Image shows an increase of ice compared to images taken earlier in the northern summer season (Figs. 2a–2c). (e) Viking Orbiter mosaic (65B56, 65B58, 65B60) acquired at a different martian year but at approximately the same time in the northern summer season ($L_s = 136$) as the image in Fig. 2d shows comparable albedo and extent of bright water ice. Visual brightness changes occur in a regular seasonal cycle rather than in an interannual cycle.

and $L_s = 136$) but different years (1978 and 1976). The low-contrast image indicates there was little albedo change from one year to the next. Due to different filters on the orbiter cameras, it is inappropriate to difference Mariner 9 and Viking Orbiter data as all color artifacts may not be eliminated. Rather, we have performed this type of analysis on Viking images only because Viking seasonal coverage is more complete. Note that the seasonal variability is visible in a much larger number of images than those presented here.

Because we consistently measured similar seasonal albedo changes in many different Viking and Mariner 9 Orbiter images, we conclude that the lack of interannual albedo variations between Mariner 9 and Viking Orbiter images is authentic. We therefore infer that processes occurred during Mariner 9 data

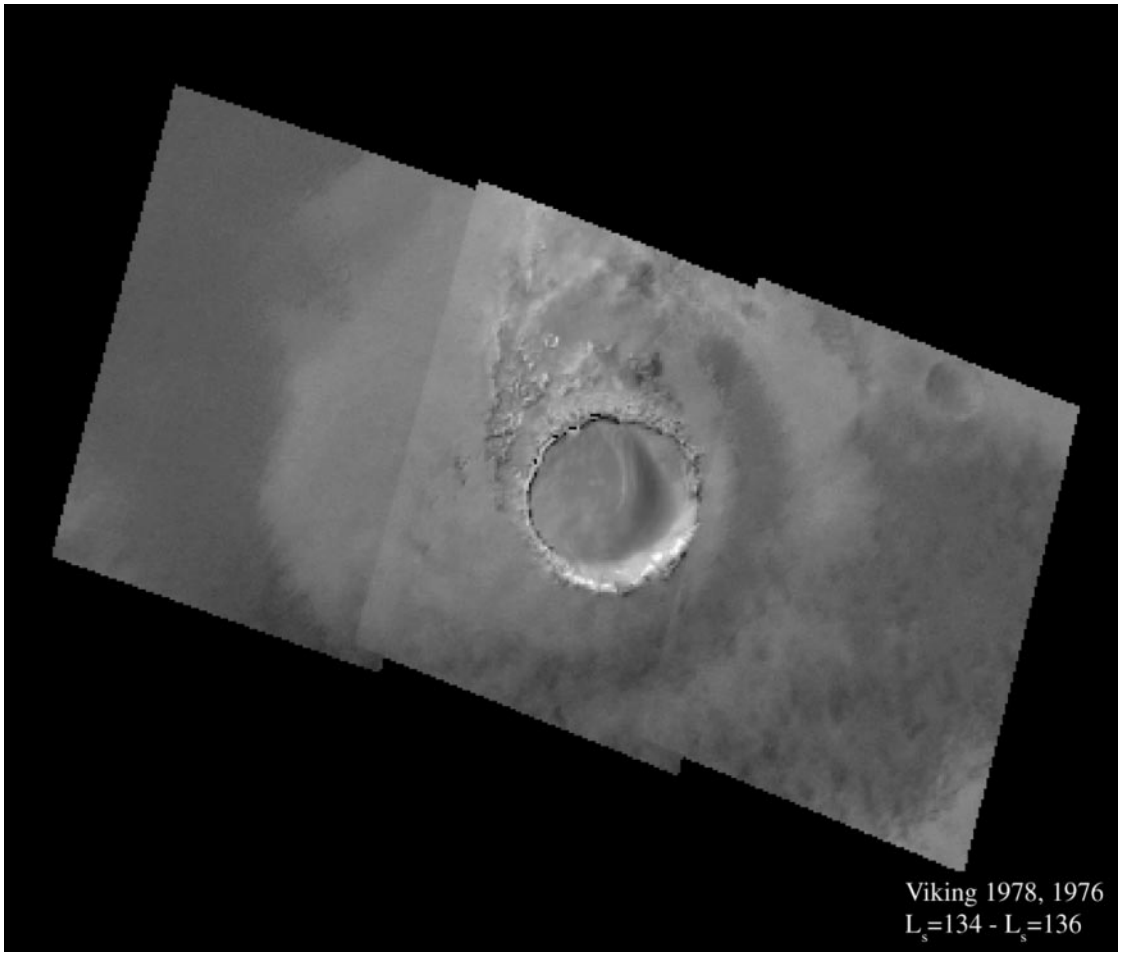

FIG. 3. Difference of two Viking images taken at approximately the same areocentric solar longitude but different martian years. The image is mostly gray, indicating that there was little contrast between the two images. The bright region in the lower right-hand portion of the crater indicates differences in shadowing in the images. Viking image 801A41 was acquired at $L_s = 134$ in 1978 and 65B56, 58, 60 were acquired at $L_s = 136$ in 1976; these images are show in Figs. 2d and 2e. All images were taken with a red filter. A linear contrast stretch was employed for DN values between 0 and 3000 and then converted to values between 0 and 255, where 0 is black and 255 is white. DN = 10,000 $*$ Lambert albedo. Emission angles for both images ranged between $\sim 75^\circ$ and $\sim 82^\circ$. Crater is 60 km across.

acquisition similar to those that occurred when the Viking data were acquired. In summary, we observed no evidence in the imaging data of large-scale interannual variability of the residual cap throughout the 4 Mars years studied.

We find that instead of an interannual variation, the albedo changes occur seasonally (Bass *et al*. 1995). North polar cap images acquired successively later in the summer show brightening in specific regions (Figs. 2b–2d). This distinct increase in albedo of certain places on the residual cap can not be attributed to the return of seasonal CO_2 ice; surface temperatures were too high at this point in the summer season (Paige and Ingersoll 1985). The large albedo increase is visible in high-and low-resolution images taken the same martian year but at increasing seasonal dates. This same seasonal albedo change can also be seen at many other cap locations (Figs. 4a–4c) and during different martian years.

Confirmation of this qualitative seasonal albedo increase can be derived from several sources. Figure 5 shows calibrated DN values from the transect in the sequence of brightening images (Figs. 2b–2d). Ice-covered locations in the images show brightening. Although data values from Fig. 2b (726A50, 52) are higher in the dark and intermediate regions in addition to the bright regions, scaling data so the dark regions overlap the dark regions of 801A41 or 765A28 (Figs. 2c and 2d) would produce an even larger difference between the bright regions of Figs. 2b and 2c. As all images were processed similarly, the brightening is not an artifact of the processing techniques. Another method of identifying quantitative differences can be found in subtraction images. Figure 6 is the difference of Figs. 2b and 2d: two images acquired at different areocentric solar longitudes ($L_s = 100$ and $L_s = 134$) in one year (1978). The large brightness contrast shows that the cap appearance altered substantially as the summer continued. In summary, each instance of supposed large-scale interannual variability reported in previous literature (James and Martin 1985, Kieffer 1990, Paige *et al*. 1994) documents changes that occur during each martian summer.

The cap is at its minimum extent and appears darkest between $L_s = 94$ and $L_s = 103$ (Figs. 1a and 2d). Interesting to note is the perpetually brighter center of the residual cap (Fig. 1a), which is located at the geographic pole. Even when the cap is at its darkest, the very center of the cap remains bright.

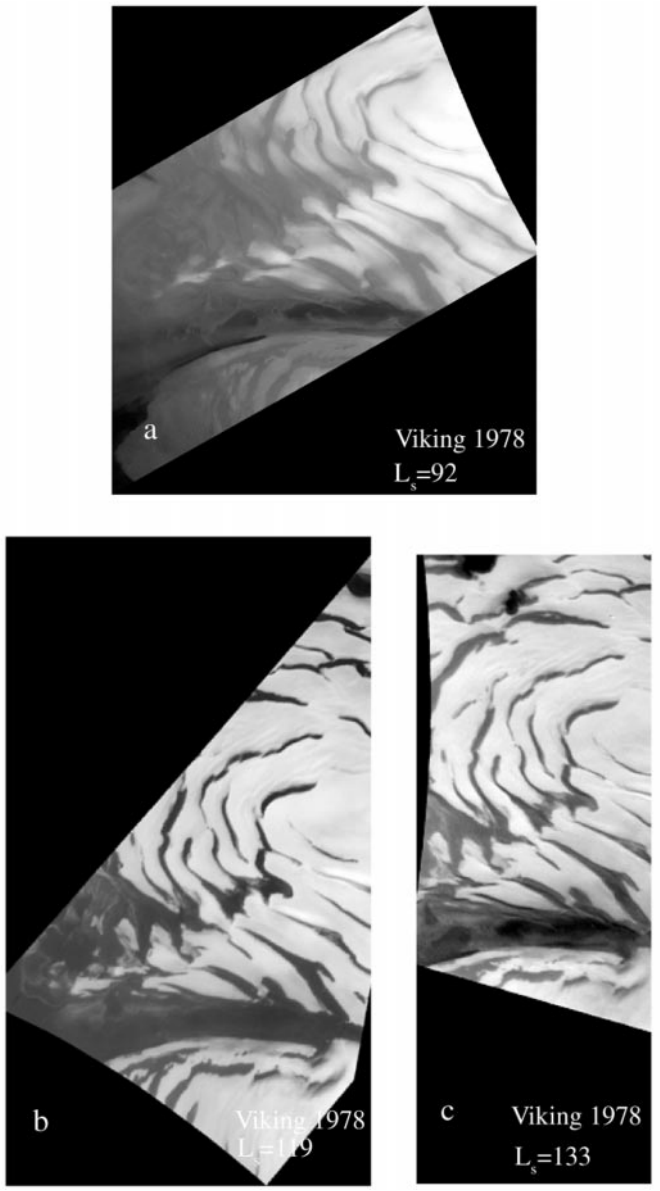

FIG. 4. Sequence of mid-resolution images increasing brightening with increasing summer season. All images have been polar-projected and have been corrected for differences in illumination using a Lambertian correction. Region in images shows approximately 82–90°N, 42–95°W. Bridge is approximately 50 km across. (a) Low-resolution Viking Orbiter image (710A76) acquired early in the northern summer season ($L_s = 92$). Note the faint outline of an "ice bridge" above Chasma Boreale, the dark re-entrant in the polar cap. Sun direction is from the lower right.(b) Viking Orbiter image (768A06) acquired later ($L_s = 119$) in the northern summer than in Fig. 4a shows distinctly more ice, again indicating that an ice increase is a seasonal phenomenon. Sun direction is from the upper right. (c) Viking Orbiter low-resolution image (797A01) acquired at $L_s = 133$. Image shows an ice bridge brighter than that visible in Viking images acquired earlier in the summer. Sun direction is from the lower right.

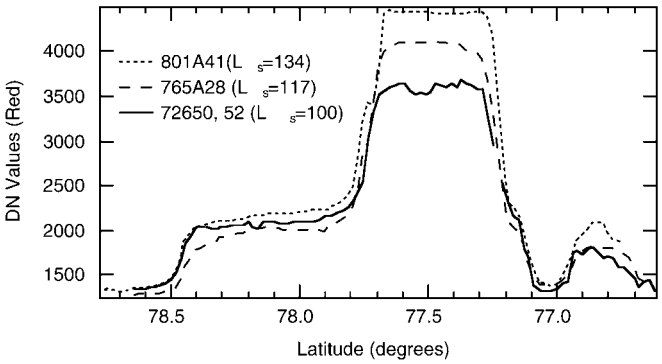

FIG. 5. Brightness from images in Figs. 2b–2d. Values plotted correspond to transect in Fig. 2b. Values from Figs. 2c–2d correspond to exact latitudes of transect in Fig. 2b. Viking images 726A50, 52 were acquired at $L_s = 100$ in 1978, image 765A28 was acquired at $L_s = 117$ in 1978, and image 801A41 was acquired at $L_s = 134$ in 1978. Increase in brightening is not an artifact of the image processing techniques; all images were corrected for illumination identically using a model Lambertian photometric correction function.

3. CHARACTERIZATION OF "NEW" LATE SUMMER ICE DEPOSITS

3.1. Previous Work

A number of possible explanations for the brightening of ice deposits in a variety of contexts have been proposed. Methods to increase the albedo of a surface deposit include ice cracking (Eluszkiewics 1993), the formation of suncups or penitentes (e.g., Lliboutry 1954), deposition of bright ice on top of a darker layer of dust, and cleaning of the dust-covered ice revealing a bright layer beneath (e.g., Hart and Jakosky 1986, Kieffer 1990). In this paper, we characterize the ice deposits and consider the possible explanations. The sensitivity of the residual polar cap and the water cycle to small amounts of water vapor may be constrained; can the deposition of only micrometers of ice (Hart and Jakosky 1986) produce extreme brightness changes on the polar cap, or are larger quantities necessary?

Assessing the amount of bright water ice that could account for the brightening in the late summer of the residual north polar cap requires an understanding of ice albedo as a function of particle size and ice deposit thickness. Wiscombe and Warren (1980) considered the albedo of a pure ice deposit by developing a model using Mie theory for single scattering coupled to a delta-Eddington approximation of radiative transfer for multiple scattering to determine ice albedo and emissivity. The Warren and Wiscombe (1980) model for the albedo of a dust-laden ice layer adapted the methods in Wiscombe and Warren (1980) and showed spectral reflectances that are in good agreement with observations of terrestrial ice deposit that are contaminated with dust and soot.

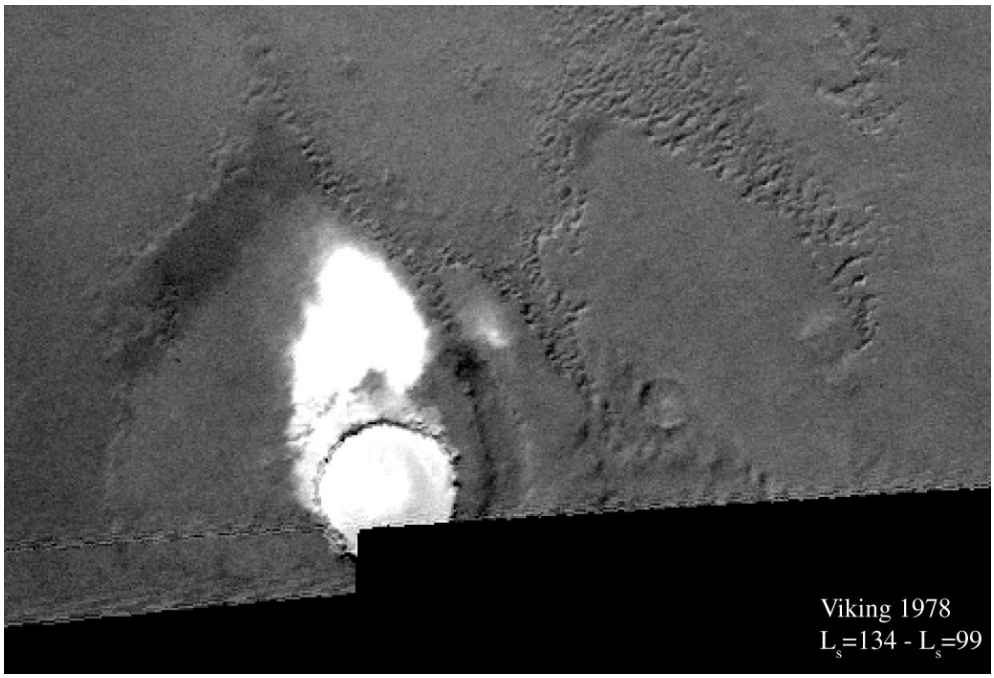

FIG. 6. Difference of two Viking images taken the same Mars year but at different times in the summer season. Viking images 726A50, 52 were acquired at $L_s = 100$ in 1978, and image 801A41 was acquired at $L_s = 134$ in 1978; Viking images are shown in Figs. 2b and 2d. All images are polar-projected and were corrected identically using a model Lambertian photometric correction function. Image has high contrast, indicating there were substantial differences in brightnesses between the two images. Crater is 60 km across.

Kieffer (1990) examined water ice grain sizes and the amount of dust that could potentially be in Mars' residual north polar cap in order to produce the observed cap albedo. Reasoning that ice grains grow larger as they age through the process of thermal metamorphism and sintering, which lowers the albedo of ice, Kieffer combined a thermal model of the residual polar cap with the Wiscombe and Warren (1980) method of determining albedo of an ice deposit given the dust content to constrain the dust/ice ratio of the residual polar cap. Ice deposits that consist of large ice particles reflect less light than ice deposits that consist of smaller ice particles due to increased multiple scattering. In order to reproduce the broad band albedo of the cap derived from spacecraft data, Kieffer concluded that the residual cap surface may consist of either older, coarse ice that must be relatively clean or else younger, fine-grained ice with a relatively higher dust content. For instance, old ice with grain sizes of 100 μm or more would have dust concentrations of 1 part per 1000 or less. With respect to the varying appearance of the residual cap different years, Kieffer (1990) suggested that dust may be removed from the surface of the cap some years. He also suggested that water may be deposited by "cold trapping" it onto the bright regions as the bright polar areas are approximately 25 K colder than the darker regions (Kieffer 1987). The observations presented in this work will be examined in light of these hypotheses.

A key issue in this study is whether the bright ice visible in the late summer has different amounts of ice and dust intimately mixed or whether there has been a change in the checkerboard pattern of deposition. Thomas and Weitz (1989) investigated the issue of mixing bright and dark material in the polar layered deposits of Mars. They estimated the amount of bright dust relative to the amount of darker "sand" by mapping the colors of the dunes in and near the polar deposits. By examining red/violet ($\lambda_{\text{eff}} = 0.59$ and $\lambda_{\text{eff}} = 0.45$) and red/green ($\lambda_{\text{eff}} = 0.59$ and $\lambda_{\text{eff}} = 0.54$) band ratio images, Thomas and Weitz (1989) concluded that there was some dark sand incorporated into the polar layered deposits, as indicated by the changing slope of the R/V ratio profiles. They used the changing ratio to indicate either a change in relative components in an intimately mixed deposit or a change in the relative checkerboard patchiness of a deposit; neither intimate mixing nor patchiness was singled out as an explanation for the distribution of ice and dust. Herkenhoff and Murray (1990) have also investigated ice/bare ground mixing in the south polar region by using ratio images.

Hart and Jakosky (1986) used spectral evidence to determine the thickness of the bright ice at the Viking Lander 2 site. They used the color of the soil relative to the nearby ice deposit to determine whether the ice was present in quantities sufficient to mask the red surface color. Hart and Jakosky (1986) estimated that a 5% increase in reflectance would result if 10 μm of ice formed on the surface. We show in the following pages that our calculations are consistent with the Hart and Jakosky (1986) estimates; 10 μm of ice may be sufficient to greatly alter the appearance of Mars' surface at the north pole.

Here we use red/violet ratios of imaging data to see if any change in ratio would indicate a change in the relative components of dust and ice in early spring ice compared to late summer ice. We do not distinguish between intimate mixing and patchy ice, but rather distinguish whether there has been a *change* in either intimate mixing or patchy ice distribution. In conjunction with this method of determining whether late summer bright ices on the residual cap have either changing amounts of intimately mixed dust and ice or changing amounts of patchy ice, we also investigate the amount of ice and dust needed to approximate the albedo seen on the cap. The amount of bright ice needed to make a previously red surface appear white has been investigated at the Viking Lander 2 site (Hart and Jakosky 1986, Svitek and Murray 1990). We apply a similar technique to bright ice on the north residual polar cap.

3.2. Determination of Ice and Dust Mixing

The Viking and Mariner 9 Orbiter imaging datasets contain information regarding the physical properties of the north polar cap surface materials. In this section, we focus on the "new" ice deposits/regions that were dark in the early summer and became bright in the late summer. To determine the mixing of bright ice and darker dust, we employ the technique of ratioing red to violet north polar region imaging data that were acquired early and also late in the northern summer season. Subsequently, we follow the methods used by Warren and Wiscombe (1980) and later adapted by Kieffer (1990) for water ice on Mars to calculate the thickness of ice deposits based on the albedo, particle size, and ice–dust mixing ratio.

3.2.1. Mixing of ice and dust results and interpretations. Image ratios like those of Thomas and Weitz (1989) quantify color differences between dark ground and bright ice within a particular image. Thomas and Weitz (1989) used the changing ratio to indicate *a change* in relative components in an intimately mixed deposit or else *a change* in the patchiness of a deposit. Figure 7 shows the range of colors of the residual cap ice on Mars. We plot a transect on Viking Orbiter image 750A23 (Fig. 7a) to identify the location of the data plotted in Fig. 7b. Figure 7b plots violet versus red Lambert albedos of two images acquired in the late northern summer season and highlights the values acquired in the region of the bright ice "bridge" that brightened in late summer. Note that the lack of significant deviation of points from a constant R/V line indicates no color differences. There is no difference in color between ice that covers the bulk of the residual cap and ice in regions that have brightened later in the northern summer. This implies that there is no detectable difference between surface material that covers the bulk of the cap and the brightened regions; there is no change in intimate mixing or change in checkerboard distribution of ice and bare ground between the different regions.

We suggest that the same processes form bright ice over the whole cap late in the summer. Further, a contiguous deposit of bright ice over the whole cap indicates that the bright ice

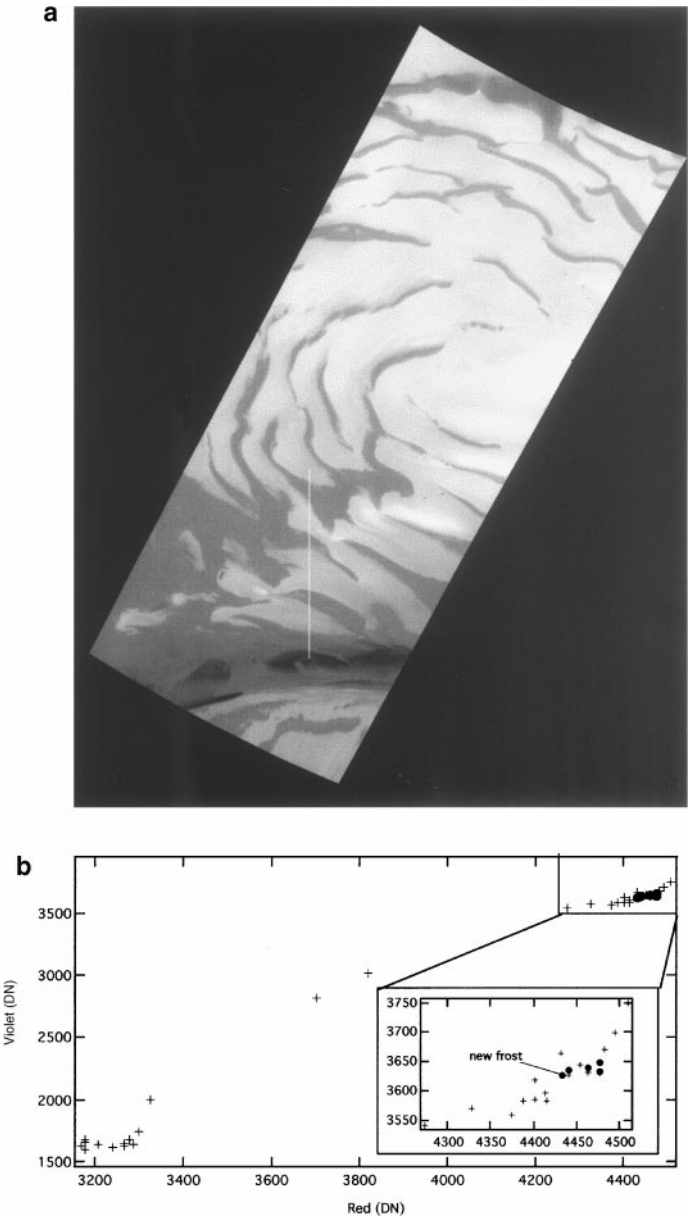

FIG. 7. Determination of color and composition of north polar ice. (a) Viking Orbiter image 750A23 acquired at $L_s = 111$. Inset shows values of newly brightened ice bridge. (b) Plot of red/violet DN values of red-filtered image 750A23 and violet-filtered image 750A26. Slope of bright ice is consistent, therefore showing little variation in color, regardless of location on the cap. Both images were corrected for illumination identically using a model Lambertian photometric correction function. A linear contrast stretch was employed for DN values between 3000 and 5000 and then converted to values between 0 and 255, where 0 is black and 255 is white. DN = 10,000 ∗ Lambert albedo.

visible in the late summer is young. Young ice indicates that it is not possible for the brightening to have been produced by the formation of either suncups or cracks in the ice as each of these mechanisms require older ice. It is also unlikely that dust would preferentially cover up only certain icy areas in the northern winter season while leaving other iced regions clear,

since the iced regions appear to have similar properties. This suggests that the residual cap ice is not translucent showing an underlying surface of dust; otherwise, variations in the deposit thickness would be apparent. Therefore, we believe the "new" ice can be treated as an optically thick layer of material overlying a darker substrate.

3.3. Albedo Calculations

The albedo of an ice deposit depends on the particle sizes of the ice, the optical properties and mixing ratio of the dark contaminants, and the ice deposit thickness. For an optically thick deposit, the minimum possible thickness can be determined from its albedo using radiative transfer theory if the particle sizes of the ice and dust are known. In our calculations, ice and dust optical properties are calculated using Mie theory, which assumes ice particles are spherical and is valid only when the distance between particles is large compared with the wavelength of the radiation. The scattering properties of dust depend strongly on the imaginary part of the complex index of refraction. The effects of close packing and nonsphericity of grains have been discussed by Wiscombe and Warren (1980) and for simplicity are not included in our calculations.

In this study, the Mie parameters for dust–ice mixtures are averaged using their respective optical cross sections per unit area as weighting factors, as

$$\frac{A_\mathrm{d}}{A_\mathrm{i}} = \left(\frac{N_\mathrm{d}}{N_\mathrm{i}}\right)\left(\frac{4\pi r_\mathrm{d}^2 Q_{\mathrm{ext_d}}\tilde{\omega}_0}{4\pi r_\mathrm{i}^2 Q_{\mathrm{ext_i}}\tilde{\omega}_0}\right) \tag{1}$$

and

$$\frac{M_\mathrm{d}}{M_\mathrm{i}} = \left(\frac{N_\mathrm{d}}{N_\mathrm{i}}\right)\left(\frac{\rho_\mathrm{d}\frac{4}{3}\pi_{r_\mathrm{d}^3}}{\rho_\mathrm{i}\frac{4}{3}\pi_{r_\mathrm{i}^3}}\right), \tag{2}$$

where M is the mass of ice or dust per square meter, N is the number density of ice grains or dust per square meter, and A is the area of ice or dust. The resulting Mie parameters are then inputs for a two-stream delta-Eddington radiative transfer calculation (Warren and Wiscombe 1980) as well as the intensity and the solar zenith angle. Hemisphere-integrated reflectance, a_s, as a function of incidence angle, is the result. In general, the albedo, a_s, depends on the optical depth, the albedo of the substrate, the solar incidence angle, the single scattering albedo ϖ_0, and the asymmetry parameter g. The optical thickness of the frost is

$$\tau_0 = N\pi r^2 Q_\mathrm{ext}, \tag{3}$$

where N is the number of particles per square centimeter and τ_0 is the optical depth. The thickness of the ice and dust deposit can be calculated from N using the respective densities of ice and dust as in Eq. (2). If the ice deposit is thick enough so that a negligible amount of radiation reaches the underlying surface and no color related to the underlying surface is visible, then the deposit can be treated as semi-infinite.

By combining the Thomas and Weitz (1989) method with the Warren and Wiscombe (1980) approach, we calculated a range of ice-and-dust depths that could be producing the albedo variations seen in the imaging data. The results are dependent upon the dust and ice optical properties. The surface (bare ground) albedo in a red band image is taken to be an average of 0.26, with a solar zenith angle of 70.0°. The density of dust is fixed at 3.0 g/cm^3, and the density of ice is taken to be the value of pure ice, 0.917 g/cm^3. We fixed dust parameters that correspond to a mean dust grain radius of 2.5 μm for these calculations. The optical constants for dust were recommended by Pollack *et al.* (1979). For $0.4 \leq \lambda \leq 1.1$ μm, the values for dust m_im were taken from Pollack *et al.* (1977) and reduced by an order of magnitude as Pollack *et al.* (1979) recommended. The justification for the use of this methodology is in keeping with properties reported in previous investigations (Pollack *et al.* 1979, Kieffer 1990). The revised Pollack *et al.* (1995) values give similar results. Changing these values (e.g., Clancy *et al.* 1995, Ockert-Bell *et al.* 1997) will not alter our results by orders of magnitude. No atmospheric correction was considered. The real index of refraction was assumed constant. A variety of ice grain radii were used, but all Mie parameters for ice are taken at 0.59-μm wavelength, which is representative of the average value in the red-filtered data. For ice, the Mie parameters were calculated using a real index of refraction equal to 1.33 and an imaginary index of refraction equal to 7.35594×10^{-9}.

3.4.1. Albedo calculations, results, and interpretations. By combining the Warren and Wiscombe (1980) calculations with our observations of a young northern water ice and the Kieffer (1990) conclusions that young ice must consist of a dusty fine-grained ice deposit, we further constrained the amount of ice that likely produced the albedo changes seen in the observations of Viking and Mariner 9 data. (Recall that ice grains grow due to sintering and metamorphosis as they age. To reproduce a particular albedo, one explanation is that ice can either be young and therefore must be fine-grained with a large component of dust or old and therefore coarse-grained with a small component of dust (Kieffer 1990).) Our results differ slightly from those of Kieffer (1990); a deposit of 50% dust should have a red albedo of 0.26 when the ice radius is 10 μm, but our calculations do not give that albedo until a much larger ice particle is employed (Fig. 8a). However, given the successful reproduction of portions of Kieffer (1990) (Fig. 8b), we feel our treatment is valid. We also show good agreement with the effect of graphitic soot on the single scattering co-albedo $(1 - \omega)$ of water ice in Warren and Wiscombe (1980). One possible explanation for the discrepancy with some of Kieffer's (1990) results is that the method presented here examines albedos in individual wavelengths rather than albedos determined from integrating across the visible spectrum, although we use the same ω_0 as Kieffer (1990); the discrepancy appeared when we moved from calculating optical parameters to incorporating the wavelengths.

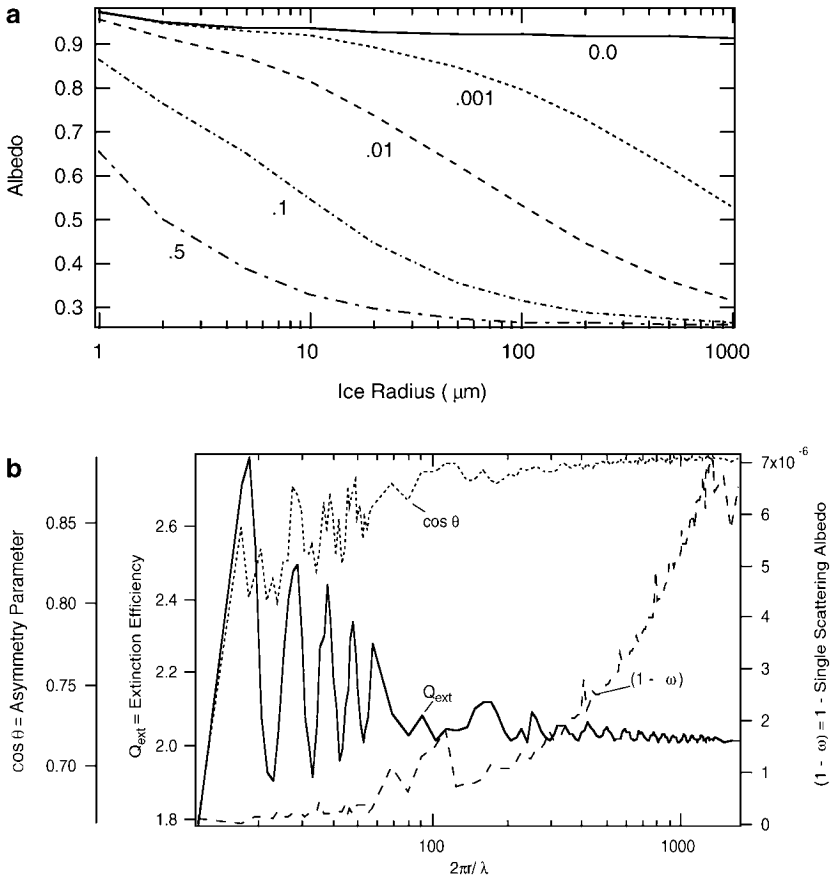

FIG. 8. Albedo of dust and ice mixture with varying mass fractions of dust. (a) Albedos calculated for this study. The dust grain radius adopted is 2.5 μm, with Q_{ext} equal to 2.74; the single scattering albedo is equal to 0.86; and the asymmetry parameter is equal to 0.79. The dust mass fraction from right to left is 0.5, 0.1, 0.01, 0.001, and 0.0. A deposit entirely of dust (mass fraction = 1.0) would have an albedo of 0.26. Albedos that correspond to particular ice radii are higher in (a) when compared to albedo values at the same ice radii in Fig. 7 of Kieffer (1990). (b) Theoretical optical scattering parameters for ice (complex index of refraction $1.311 + (3.1 \times 10^{-9})i$ and wavelength 0.55 μm) computed using Mie scattering theory.

We present calculations of the range of dust and ice grain sizes that can produce the albedo variations noted in Figs. 2a–2e (Fig. 9). A semi-infinite layer corresponds to a large optical depth (τ), which provides a lower constraint on the amount of dust and ice present in the ice layer. From these plots, we determined that a red Lambert albedo of 0.33–0.35, the maximum albedo of the ice in Viking image 750A23 (Fig. 7a), can be produced by an ice deposit with either 50% dust and ice radii of 10 μm or 10% dust with 50 μm ice radii or smaller components of dust (1%) with larger ice grains (500 μm) (Fig. 9). As shown in Fig. 9, values that corresponded to an albedo of 0.33 to 0.35 as stated above and an opacity greater than 2 were adopted, because at opacities lower than this value the ice layer is not yet semi-infinite optically. These correspond to ice and dust mixtures deposited on the cap of 14 precipitable μm, 35 precipitable μm, and 300 precipitable μm of ice and dust, respectively. Note that these values are dependent on the dust and ice optical properties and represent the minimum amount of ice that can reproduce the observed albedos; it is possible that much more ice was deposited at these sites. Indeed, it is likely that more ice was deposited in the first two cases, as the layer thicknesses are less than the grain sizes.

4. CONCLUSIONS

4.1. Residual Cap Appearance

To summarize, the available Mariner 9 and Viking Orbiter images suggest the following regarding the appearance of the residual cap:

1. There is no large-scale variation of the residual cap appearance from year to year.
2. The cap is darkest between $L_s = 94$ and $L_s = 103$.
3. There is a seasonal variation in the residual cap appearance: in general, the entire residual cap grows brighter as the summer progresses.

4. Specific outlying cap regions that are dark in the beginning of the summer brighten every year by the end of the summer season.

5. The bright outliers consistently have the same shapes at the end of each summer.

6. The residual cap center is always brighter than the cap edges.

These observations lead us to conclude that the residual cap appearance was not, to a great extent, affected by the interannually occurring global dust storms, at least during the 3 Mars years observed. This implies that the same processes act on the residual cap each year. Perhaps the same deposition and erosion of the cap occurs each year at the present obliquity, and global dust storms have a much smaller effect on ice deposition than previously thought.

The bright permanent ice deposits in the north polar region may be acting as "cold traps" which cause bright water ice to accumulate on their surfaces when water passes over these deposits. Therefore, the residual cap appearance is primarily affected by albedo and local temperatures, indicating that these effects must be treated with care when modeling the water cycle on Mars. In addition to the regular seasonal variation of the water cycle in the north polar region, it appears the residual cap acts as a cold trap for water vapor in the summer.

The late summer-brightened cap outliers seem to follow the same patterns or outlines from year to year, leading us to believe that these regions must always be cold relative to the surrounding bare ground and trap bright ice in the same area each year. A positive feedback could be maintaining the distribution of the ice, enhanced by topography. These observations strongly suggest that these regions are acting as cold traps for bright water ice in the summer season. It does not seem likely that dust would be preferentially removed from only certain areas of the residual cap and that these areas are cleaned in exactly the same fashion with no change in visual appearance every year. Therefore, we believe new ice deposition on the residual north polar cap is the most probable explanation for the late summer cap brightening.

The maximum observed brightness of the peripheral regions examined was significantly lower than albedos measured at the center of the residual cap (Figs. 1a and 7b). The cap center is likely brighter than the cap edge because ice annually accumulates there and is younger than the ice at the cap edges. Therefore, observations concerning the cap center are not necessarily representative of the entire cap. The perpetually bright center of the north residual polar cap (Fig. 1a) may indicate that at least the cap center is acting as a net sink for water vapor; the brightness is consistent with active accumulation in this region through most of the summer season. It seems logical that if dark areas are seasonally accumulating ice such as in Fig. 2, it is likely that the brighter areas that act as cold traps are also regions of seasonal accumulation. Each year approximately the same amount of ice appears to be deposited and removed from the bulk of the residual cap, with the exception of possible accumulation of water ice at the cap center. This indicates that the uppermost layer of the residual cap may represent current climatic conditions; water may be cycled from the cap edges to the center each summer.

4.2. Characterization of New Late Summer Ice Deposits

Regarding the ice deposits, we find:

1. The bright ice that appears in the late summer on the cap outliers is the same color as the ice on the rest of the cap.

2. Assuming dust radii of 2.5 μm, the maximum albedo of the late summer ice corresponds to an ice deposit of at least (a) 50% dust with ice radii of 10 μm, (b) 10% dust with ice radii of 50 μm, or (c) 1% dust with ice radii of 500 μm.

3. The amount of deposited dust and ice must be greater than 14 pr μm for a deposit with smaller sized grains or else greater than 35 pr μm for a deposit with larger sized grains.

Recall that a difference in red to violet ratios would indicate either a change in the amount of dust relative to ice in the deposit or a checkerboard distribution of ice and dust. Our findings indicate that there is no difference in the relative amounts of ice and dust (no *change* in intimate mixing or *change* in checkerboard distribution of ice) in the bright ice outliers that appear in late summer relative to the rest of the cap because the red component of the ratioed images relative to the violet component remains constant (Figs. 7a–7c). Also, since bright ice that appears in the late summer has the same R/V ratio as ice on the rest of the cap, the processes that produce the bright ice on the bulk of the cap are probably the same as those producing the late summer-brightened outliers. Although this cannot be determined conclusively, we also point out that because it is highly unlikely that all of the ice on the main cap would be equally as patchy as the smaller outliers, it is possible that the late summer ice producing the brightened albedo is not arranged in a checkerboard distribution.

The brightened regions most likely consist of young ice deposited late in the summer. Following Kieffer's suggestions, this indicates that the ice must be relatively fine-grained, but to produce the observed cap albedo it must also be relatively dust-rich. To produce such an albedo change, the cap surface must be relatively smooth; highly varying topography would produce patchy ice coverage on observable lengthscales. This observation is consistent with the Simpson and Tyler (1981) bi-static radar observation which showed that the residual north polar cap is relatively smooth on centimeter to meter lengthscales.

As previously mentioned, because the ice appeared later in the season and had the same composition and color as the bulk of the residual cap, it is likely young and consists of a dust-laden, fine-grained deposit (Thomas and Weitz 1989, Kieffer 1990). Therefore, a deposit composed of only 1% dust is unlikely. A deposit thickness of at least 14 μm or at least 35 μm (Figs. 9b and 9c) is consistent with the Hart and Jakosky (1986) estimates of

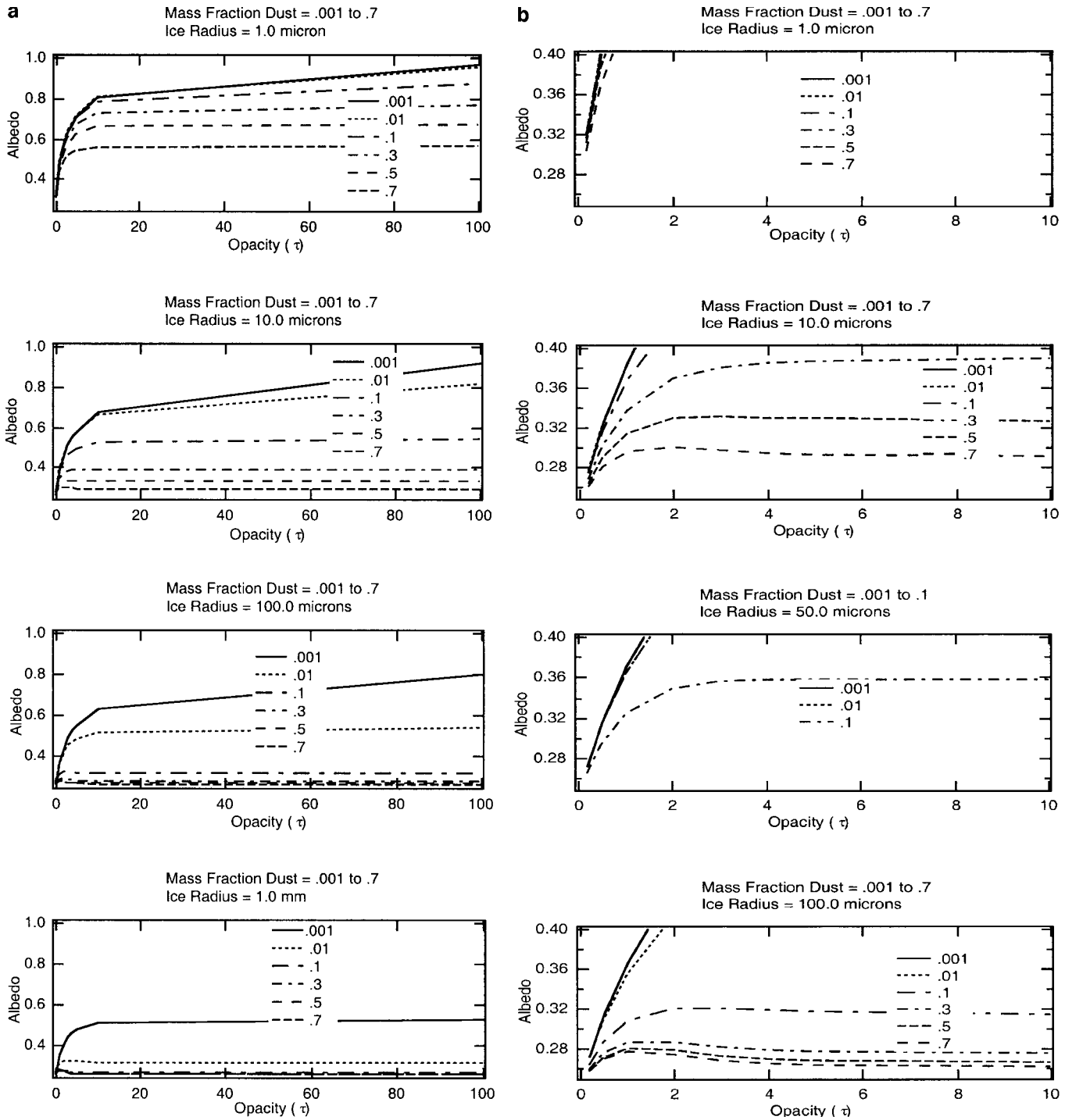

FIG. 9. Brightness of ice deposit as a function of opacity. Albedos and opacities shown reproduce an albedo of approximately 0.34, the maximum albedo in Fig. 8a. Albedos that corresponds to opacities of 2 to 3 are considered when determining ice deposition amounts as these albedos correspond to a "semi-infinite" layer of ice and dust. (a) "Mass fraction dust" refers to the amount of dust in the deposit, e.g., 0.1% dust, 1.0% dust. Surface albedo defined as 0.24. Note inflection points move toward lower opacities as shown in top graph. Ice depths represent a "semi-infinite" layer, which corresponds to opacities that are asymptotic. (b) Albedos and opacities shown are more resolved views of Fig. 9a. Albedos that corresponds to opacities of 2 to 3 are considered when determining ice deposition amounts as these albedos correspond to a "semi-infinite" layer of ice and dust. (c) Albedos and opacities shown represent particle sizes larger than those in Figs. 9a and 9b.

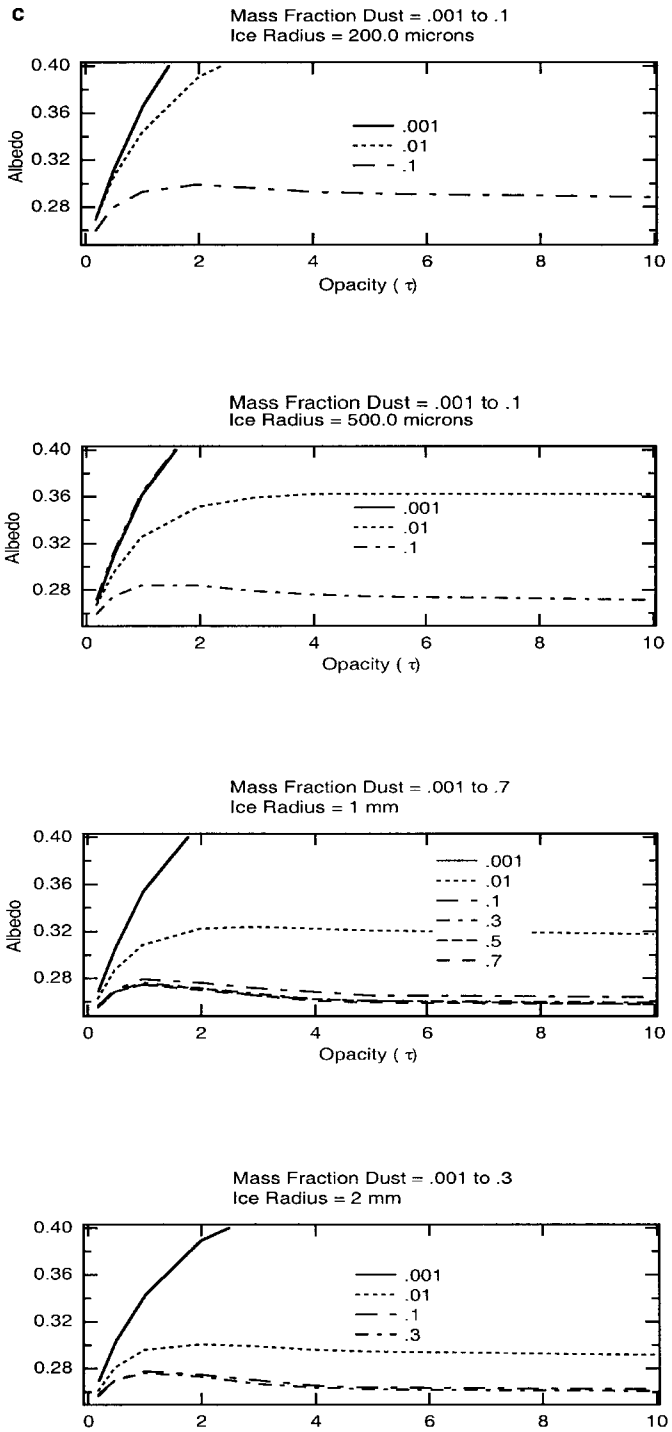

FIG. 9—*Continued*

approximately 10 μm of ice deposited at the Viking Lander 2 site and implies that a very small amount of deposited ice was responsible for the observed change in the appearance of the residual cap.

Because the large-scale appearance of the cap does not seem to vary from year to year, it is reasonable to assume that the same amount of ice is deposited on the cap surface each summer season. However, this does not necessarily imply that there is an annual net deposition of ice. In fact, it is possible that while deposition occurs at the center of the cap, there is also some transport of water vapor away from the cap (Haberle and Jakosky, 1990). Without more data, this leaves the issue of the net annual water balance on the cap as a whole highly uncertain.

ACKNOWLEDGMENTS

We thank Bruce Jakosky and Francois Forget for reviews of an earlier version of the manuscript; we also thank an anonymous reviewer for helpful comments. This research was supported by the National Aeronautics and Space Administration under Grant NAGW 4327 and by the NASA Graduate Student Researchers Program, NGT-51273.

REFERENCES

Bass, D. S., and D. A. Paige 2000. Variability of Mars' north polar water ice cap. II. Analysis of Viking IRTM and MAWD data. *Icarus* **144**, 397–409.

Bass, D. S., K. E. Herkenhoff, and D. A. Paige 1994. Variations in Mars' north residual polar cap frost coverage in Mariner 9 and Viking images. *Proc. Lunar Planet. Sci. Conf. 25th*, 69–70.

Bass, D. S., D. A. Paige, and K. E. Herkenhoff 1995. Variability of Mars' north polar cap water frost: Interannual or seasonal? *Bull. Am. Astron. Soc.* **27**, 38.

Bills, B. G. 1990. The rigid body obliquity history of Mars. *J. Geophys. Res.* **95**, 14,137–14,153.

Blasius, K. R., J. A. Cutts, and A. D. Howard 1982. Topography and stratigraphy of martian polar layered deposits. *Icarus* **50**, 140–250.

Clancy, R. T., S. W. Lee, G. R. Gladstone, W. W. McMillan, and T. Roush, 1995. A new model for Mars's atmospheric dust based upon analysis of ultraviolet through infrared observations from Mariner 9, Viking, and Phobos. *J. Geophys. Res.* **100**, 5251–5263.

Cutts, J. A. 1974. Mariner Mars 1971 television picture catalog. *NASA Tech. Memor.* 33–85.

Cutts, J. A., K. R. Blasius, and W. J. Roberts 1979. Evolution of martian polar landscapes: Interplay of long-term variations in perennial ice cover and dust storm intensity. *J. Geophys. Res.* **84**, 2975–2994.

Eluszkiewics, J. 1993. On the microphysical state of the martian seasonal caps. *Icarus* **103**, 43–48.

Fanale, F. P., S. E. Postawko, J. B. Pollack, M. H. Carr, and R. O. Pepin 1992. Mars: Epochal climate change and volatile history. *In Mars* (H. H. Kieffer, B. M. Jakosky, C. W. Snyder, and M. S. Matthews, Eds.), pp. 1135–1179. Univ. of Arizona Press, Tucson.

Farmer, C. B., D. W. Davies, and D. D. La Porte 1976. Viking: Mars atmospheric water vapor mapping experiment—Preliminary report of results. Science **193**, 776–780.

Haberle, R. M., and B. M. Jakosky 1990. Sublimation and transport of water from the north residual polar cap of Mars. *J. Geophys. Res.* **95**, 1423–1437.

Hart, H. M., and B. M. Jakosky 1986. Composition and stability of the condensate observed at the Viking Lander 2 site on Mars. *Icarus* **66**, 134–142.

Herkenhoff, K. E., and B. C. Murray 1990. Color and albedo of the south polar layered deposits on Mars. *J. Geophys. Res.* **95**, 1343–1358.

Herkenhoff, K. E., L. A. Soderblom, B. C. Murray, and G. E. Danielson 1988. Mariner 9 television calibration—Revisited. *Icarus* **75**, 133–145.

Hofstadter, M. D., and B. C. Murray 1990. Ice sublimation and Rheology: Implications for the martian polar layered deposits. *Icarus* **84**, 352–361.

Houben, H., R. M. Haberle, R. E. Young, and A. Zent 1997. Modeling the martian water cycle. *J. Geophys. Res.* **102**, 9069–9084.

Howard, A. D., J. A. Cutts, and K. J. Blasius 1982. Stratigraphic relationships within the martian polar cap deposits. *Icarus* **50**, 161–215.

Imbrie, J. 1982. Astronomical theory of the Pleistocene ice ages—A brief historical review. *Icarus* **50**, 408–422.

Jakosky, B. M., and E. S. Barker 1984. Comparison of ground-based measurement of martian water vapor: Variability of the seasonal cycle. *Icarus* **57**, 322–334.

Jakosky, B. M., and C. B. Farmer 1982. The seasonal and global behavior of water vapor in the Mars atmosphere: Complete global results of the Viking Atmospheric Water Detector Experiment. *J. Geophys. Res.* **87**, 2999–3019.

Jakosky, B. M., and R. M. Haberle 1992. The seasonal behavior of water on Mars. *In Mars* (H. H. Kieffer, B. M. Jakosky, C. W. Snyder, and M. S. Matthews, Eds.), pp. 969–1016. Univ. of Arizona Press, Tucson.

James, P. B. 1979. Recession of martian north polar cap. *J. Geophys. Res.* **84**, 8332–8334.

James, P. B., and L. Martin 1985. Interannual water loss by Mars' north polar cap. *Bull. Am. Astron. Soc.* **17**, 735.

Jouzel, J., C. Lorius, J. R. Petit, C. Genthon, N. I. Markov, V. M. Kotlyakov, and V. M. Petrov 1987. Vostok ice core: A continuous isotope temperature record over the last climatic cycle (160,000 years). *Nature* **329**, 403–408.

Kahn, R. A. 1990. Ice haze, snow, and the Mars water cycle. *J. Geophys. Res.* **95**, 14,677–14,693.

Kahn, R. A., T. Z. Martin, R. W. Zurek, and S. W. Lee 1992. The martian dust cycle. In *Mars* (H. H. Kieffer, B. M. Jakosky, C. W. Snyder, and M. S. Matthews, Eds.), pp. 1017–1053. Univ. of Arizona Press, Tucson.

Kieffer, H. H. 1987. How dirty is Mars' north polar cap, and why isn't it black? In *MEVTV Workshop on Nature and Composition of Surface Units on Mars* (SEE N88-2965423-91), pp. 72–73. Lunar Planetary Institute, Houston.

Kieffer, H. H. 1990. H_2O grain size and amount of dust in Mars' residual north polar cap. *J. Geophys. Res.* **96**, 1481–1493.

Kieffer, H. H., S. C. Chase, Jr., T. Z. Martin, E. D. Miner, and F. D. Palluconi 1976. Martian north pole summer temperatures: Dirty water ice. *Science* **194**, 1341–1344.

Kieffer, H. H., T. Z. Martin, A. R. Peterfreund, B. M. Jakosky, E. D. Miner, and F. D. Palluconi 1977. Thermal and albedo mapping of Mars during the Viking primary mission. *J. Geophys. Res.* **82**, 4249–4291.

Klaasen, K. P., T. E. Thorpe, and L. A. Morabito 1977. Inflight performance of the Viking visual imaging subsystem. *Appl. Opt.* **16**, 3158–3170.

Lliboutry, L. 1954. The origin of penitents. *J. Glaciol*. **2**, 331–338.

Murray, B. C., W. R. Ward, and S. C. Yeung 1973. Periodic insolation variations on Mars. *Science* **180**, 638–640.

Ockert-Bell, M. E., J. F. Bell III, J. B. Pollack, C. P. Mckay, and F. Forget 1997. Absorption and scattering properties of the martian dust in the solar wavelengths. *J. Geophys. Res*. **102**, 9039–9050.

Paige, D. A., and A. P. Ingersoll 1985. Annual heat balance of martian polar caps: Viking observations. *Science* **228**, 1160–1168.

Paige, D. A., J. E. Bachman, and K. E. Keegan 1994. Thermal and albedo mapping of the polar regions of Mars using Viking thermal mapper observations. 1. North polar region. *J. Geophys. Res.* **99**, 25,959–25,991.

Pollack, J. B., D. S. Colburn, F. M. Flasar, R. Kahn, C. E. Carlson, and D. Pidek 1979. Properties and effects of dust particles suspended in the martian atmosphere. *J. Geophys. Res.* **84**, 2929–2945.

Pollack, J. B., D. Colburn, R. Kahn, J. Hunter, W. Van Camp, C. E. Carlson, and M. R. Wolf 1977. Properties of aerosols in the martian atmosphere, as inferred from Viking Lander imaging data. *J. Geophys. Res.* **82**, 4479–4496.

Pollack, J. B., M. E. Ockert-Bell, and M. K. Shepard 1995. Viking Lander image analysis of martian atmospheric dust. *J. Geophys. Res.* **100**, 5235–5250.

Simpson, R. A., and G. L. Tyler 1981. Viking bistatic radar experiment: Summary of first-order results emphasizing north polar data. *Icarus* **46**, 361–389.

Slavney, S. H., and E. A. Guinness 1989. Image Retrieval and Processing System (IRPS) Software Specification Document. Washington University, St. Louis.

Svitek, T., and B. Murray 1990. Winter frost at Viking Lander 2 site. *J. Geophys. Res*. **95**, 1495–1510.

Thomas, P., and C. Weitz 1989. Sand dune materials and polar layered deposits on Mars. *Icarus* **81**, 185–215.

Touma, J., and J. Wisdom 1993. The chaotic obliquity of Mars. *Science* **259**, 1294–1297.

Ward, W. R. 1992. Long-term orbital and spin dynamics of Mars. *In Mars* (H. H. Kieffer, B. M. Jakosky, C. W. Snyder, and M. S. Matthews, Eds.), pp. 298–320. Univ. of Arizona Press, Tucson.

Warren, S. G., and W. J. Wiscombe 1980. A model for the spectral albedo of snow. II. Snow containing atmospheric aerosols. *J. Atmos. Sci*. **37**, 2734–2745.

Warren, S. G., W. J. Wiscombe, and J. F. Firestone 1990. Spectral albedo and emissivity of CO_2 in martian polar caps: Model results. *J. Geophys. Res.* **95**, 14,714–14,741.

Wiscombe, W. J., and S. G. Warren 1980. A model for the spectral albedo of snow. I. Pure snow. *J. Atmos. Sci*. **37**, 2712–2722.

Zent, A. P., F. P. Fanale, J. R. Salvail, and S. E. Postawko 1986. Distribution and state of H_2O in the high-latitude shallow subsurface of Mars. *Icarus* **67**, 19–36.

Zurek, R. W., and L. J. Martin 1993. Interannual variability of planet-encircling dust storms on Mars. *J. Geophys. Res.* **98**, 3247–3260.